Focused ion beam milling of microchannels in lithium niobate

Manoj Sridhar,[1,a)] Devendra K. Maurya,[1,2] James R. Friend,[1,2,b)] and Leslie Y. Yeo[1,2,b)]

[1]*Melbourne Centre for Nanofabrication, Clayton VIC, Australia*
[2]*Micro/Nanophysics Research Laboratory, Department of Mechanical and Aerospace Engineering, Monash University, Clayton VIC, Australia*

We present experimental and simulation results for focused ion beam (FIB) milling of microchannels in lithium niobate in this paper. We investigate two different cuts of lithium niobate, *Y*- and *Z*-cuts, and observe that the experimental material removal rate in the FIB for both *Y*-cut and *Z*-cut samples was 0.3 μm^3/nC, roughly two times greater than the material removal rate previously reported in the literature but in good agreement with the value we obtain from stopping and range of ions in matter (SRIM) simulations. Further, we investigate the FIB milling rate and resultant cross-sectional profile of microchannels at various ion beam currents and find that the milling rate decreases as a function of ion dose and correspondingly, the cross-sectional profiles change from rectangular to V-shaped. This indicates that material redeposition plays an important role at high ion dose or equivalently, high aspect ratio. We find that the experimental material removal rate decreases as a function of aspect ratio of the milled structures, in good agreement with our simulation results at low aspect ratio and in good agreement with the material removal rates previously reported in the literature at high aspect ratios. Our results show that it is indeed easier than previously assumed to fabricate nanochannels with low aspect ratio directly on lithium niobate using the FIB milling technique. © *2012 American Institute of Physics*. [doi:10.1063/1.3673260]

I. INTRODUCTION

Lithium niobate (LN) represents the most common piezoelectric material used in radio-frequency (RF) telecommunications[1,2] including mobile phones, television, and wireless transmitters, a technology that has become a fixture in nearly every person's life worldwide. While other piezoelectric materials offer certain advantages in other applications,[3] single-crystal LN offers the highest electromechanical coupling of any available material over the RF range in the 127.68° *Y*–axis rotated, *X*–axis propagating surface acoustic wave.[4] Furthermore, in optical applications, LN offers powerful electro-optical coupling as well[5] with the *Y* and *Z* cuts, and advances in use of the material continue with the application of periodically poled LN.[6]

In recent years, piezoelectrically generated acoustic energy has been found to be extremely useful for microfluidics in a broad range of applications,[7,8] from atomisation for drug delivery[9,10] to fluid jetting,[11] microcentrifugation,[12] microfluidic pumping,[13] particle concentration and mixing in microdrops,[14] micro/nanoparticle generation,[15,16] biological cell manipulation,[17] and tissue engineering.[18] Because of the micrometer-order dimensions of these applications and the need for acoustic energy sources compatible with the planar geometry typical of microfabricated fluidics devices, acoustic waves in the form of *surface acoustic waves* (SAW) in LN at frequencies from 5 MHz to a few GHz are ideal.

[a)]Author to whom correspondence should be addressed. Electronic mail: manoj.sridhar@monash.edu.
[b)]Present address: Micro/NanoPhysics Research Laboratory, RMIT University, Melbourne VIC 3001, Australia.

Unfortunately, machining LN, whatever the cut, is a difficult matter. Easily fractured and very anisotropic, highly pyroelectric, inert to most etchants, and transparent to all but shortest wavelengths of lasers (for instance, LN can be machined using a 289 nm exciplex UV laser[13]), LN has traditionally been left as an inert substrate upon which electrodes, functional materials and microfluidics structures are deposited, and mechanically diced to provide finished devices. Focused ion beam (FIB) machining is a viable alternative, having been used to machine LN in limited studies in the past.[19–25] It is perhaps an ideal choice now that its material removal rates have been increased to $0.3 \, \mu m^3$/nC and the lower resolution limit has decreased to 100 nm.

Although much of the potential in microfluidics devices using acoustics has yet to be realised, the use of acoustic waves at the nano-scale cannot be underestimated. Already, the evidence is clear—in Edel *et al.*,[26] for example—that fluidics phenomena at the nano-scale is far different than at larger scales, and that exploiting such phenomena will yield unprecedented technologies just as what has happened in microfluidics. Given the apparently peculiar, non-Fickian nature of fluid flow at the nano-scale,[27] it is perhaps no surprise that phonon transport in nanoscale structures with fluids adjacent to them would result in interesting behaviour. Insepov and his colleagues[28] report that if one were to use surface acoustic waves transmitted along carbon nanotubes, the peristaltic motion that occurs along the nanotubes would be sufficient to pump gases beyond 30 km/s along their length, though the frequencies necessary to actually deliver reasonable flow rates of around 10 cc/min appear to be well into the THz range for their 100 Å-long nanotube. Notwithstanding the many assumptions in their analysis and the inherent problems in using molecular dynamics solutions to interpret the probable behaviour of real systems over physically meaningful time scales, the work and the tantalising results of other groups[29] indicate the potential of acoustics as a useful means to provide fluid motion well into the future, particularly in water purification.[30] The non-Newtonian behavior of fluids at the nano-scale is yet another intriguing line of possible investigation.[31]

Curiously, though FIB has been used to machine LN in the past, no comprehensive study on the process has been made, and the results reported in the literature appear to conflict with each other. Due to the potential for FIB in addressing the absence of effective machining methods for LN, especially for submicron features, this oversight needs to be addressed. In this paper, we present a comprehensive study of the FIB milling technique for fabricating a wide range of structures and show that FIB milling of nanochannels on lithium niobate, to go beyond microfluidics towards *nano*fluidics: fluid transport in structures with characteristic length scales of 100 nm could be easier than previously assumed.

II. EXPERIMENTAL METHODS

127.68° axis rotated *Y*-cut (SAW grade) and *Z*-cut LN wafers were obtained from Roditi International Corporation and diced into approximately 10 mm by 10 mm square samples. The LN samples were then coated with a thin layer (about 25 nm) of gold by thermal evaporation to act as a conducting layer to avoid charging effects and facilitate ion milling and scanning electron microscopy (SEM) imaging.

All FIB milling experiments were conducted on the LN samples using a FEI Helios NanoLab 600 DualBeam FIB-SEM. Ga^+ ions are emitted with an accelerating voltage of 30 kV at normal incidence to the sample surface. The ion beam overlap was fixed to the default value of 50% for all experiments, i.e., the beam was moved through the mill area in steps equal to half the beam diameter at a particular current, to minimize the effect of the Gaussian profile of the ion beam on the profile of the milled channels. All channels were first milled, in triplicate for better statistics, sequentially using the FIB, cross-sections were then cut using the FIB with a lower ion beam current than the current used to mill the channel, and finally, the milled channels were imaged and the dimensions were measured using the SEM *in situ*. Image analysis software available with the FEI xT user interface was then used to determine the cross-sectional area of the milled channel. This value was then multiplied by the length of the milled channel to determine the total milled volume.

III. EXPERIMENTAL AND SIMULATION RESULTS

A. Material removal rate for Y- and Z-cuts LN in the FIB

Channels with six different volumes varying from about 50-250 μm^3 were milled in triplicate using the FIB in both *Y*- and *Z*-cuts LN samples. Each milled channel was cross-sectioned using the FIB and the dimensions of the milled channels were measured in the SEM. Figure 1 shows a SEM image of the cross-section of a typical FIB-milled channel.

The channel shown in Figure 1 was milled in a *Z*-cut LN sample and is about 2 μm wide and 600 nm deep. Due to the Gaussian nature of the FIB, some of the Au conducting layer surrounding the channel also appears to have been sputtered away during the milling process, as is evidenced by the thin gray halo region around the milled channel. The step structures that are visible in Figure 1 are standard features created during the process of cross-sectioning the channel in the FIB. The volume of each of the milled channels was then calculated by using the measured dimensions and plotted against the total Ga$^+$ charge incident on each channel for both the *Y*- and *Z*-cuts samples in Figure 2.

As expected, the volume of LN that is sputtered away varied linearly with the number of Ga$^+$ ions incident on the surface of the sample for both *Y*- and *Z*-cut samples. The gradient of a linear fit through each set of data points gives us the value for the material removal rate for each cut of LN. Using this method, we obtain an experimental material removal rate of 0.34 ± 0.02 μm^3/nC for *Y*-cut samples and 0.30 ± 0.02 μm^3/nC for *Z*-cut samples. Thus, we observe that there is no significant dependence of the material removal rate using the FIB on the surface orientation of LN.

Table I shows a list of material removal rates using the FIB reported by various researchers[19,21–25] for different cuts of LN. The geometry of the structures milled by Lacour *et al.*[19] and Sulser *et al.*[23] is not entirely clear, and hence, there are a range of material removal rates (0.05–0.15 and 0.07–0.22 μm^3/nC, respectively) that we have inferred from their paper. Also, Xu *et al.*[24] and Liu *et al.*[25] milled a number of structures with different geometries, and therefore, we have listed the reported range of material removal rates (0.13–0.19 and 0.10–0.12 μm^3/nC, respectively).

From this table, we can see that we have achieved a material removal rate in the FIB for LN roughly two times greater than has been previously reported. It must be noted that previous reports of FIB milling of LN have focused on milling arrays of cylindrical or conical holes in the substrate for optical applications, i.e., structures with high aspect ratio. In fact,
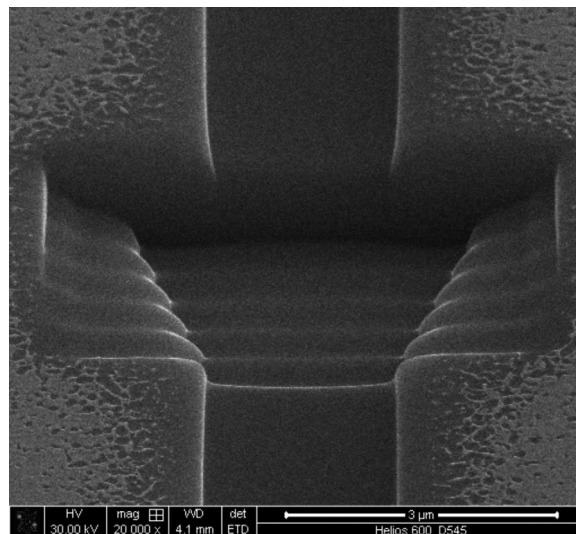

FIG. 1. SEM image of the cross-section of a typical FIB-milled channel in LN. In this case, the milled channel was 2 μm wide and 600 nm deep, the substrate was *Z*-cut LN, and the bright area surrounding the milled channel is the 25 nm Au conducting layer.
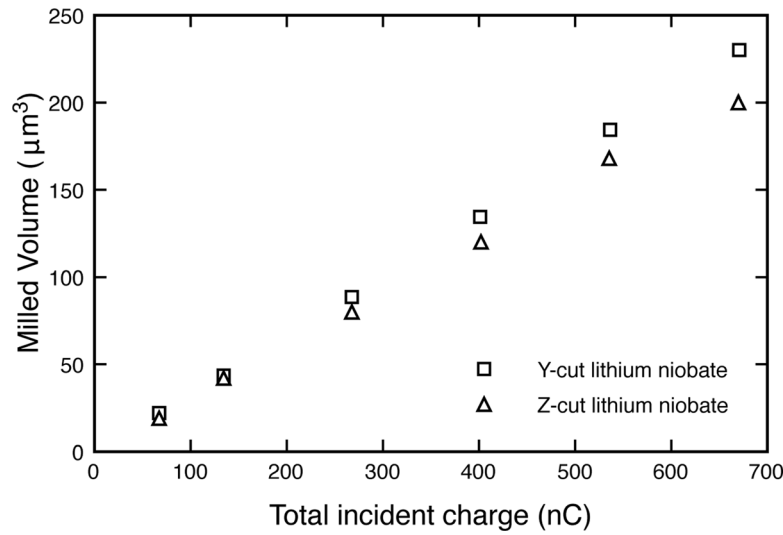
FIG. 2. Plot of average milled volume of microchannels (as measured in the SEM) as a function of total incident Ga$^+$ charge for *Y*- and *Z*-cuts LN.

Roussey *et al.*,[21] Xu *et al.*,[24] and others have claimed that they observe significant material redeposition, which is common and significant when milling high aspect ratio structures, thus limiting the material removal rate that they are able to achieve.

B. SRIM simulation results

We performed Monte Carlo simulations using the popular SRIM-2011 program[32] to obtain a theoretical estimate of the material removal rate of lithium niobate using the FIB with 30 keV Ga$^+$ ions normally incident to the sample surface. SRIM-2011 determines the stopping power, range, and sputter yield of ions using a quantum mechanical treatment of ion-target collisions. A detailed description of the calculation can be found elsewhere.[32] We used the LN compound listed in the standard compound listings of SRIM-2011 with a value of 4.628 g/cm^3 for the density of lithium niobate.[36] The important parameters used in our simulations are listed in Table II.

We simulated 10 000 Ga$^+$ ions impinging on the LN surface to minimise statistical error in the simulations and the results for the sputter yield of each type of atom, i.e., the number of atoms removed from the substrate surface per impinging Ga$^+$ ion, we obtained are reported in Table III.

From this data, we were able to calculate the total mass lost from the lithium niobate substrate due to sputtering. Using the same density of lithium niobate as used in the SRIM simulations (4.628 g/cm^3), we calculated a theoretical material removal rate of 0.37 μm^3/nC based on

TABLE I. Material removal rates using the FIB reported by various research groups, including our results reported here, for different cuts of LN.

Reference	Cut	Material removal rate (μm^3/nC)
This paper	*Y*-cut	0.34
This paper	*Z*-cut	0.30
Lacour *et al.* (Ref. 19)	*Z*-cut	0.05–0.15
Liu *et al.* (Ref. 25)	*Z*-cut	0.10–0.12
Roussey *et al.* (Ref. 21)	*X*-cut	0.15
Bernal *et al.* (Ref. 22)	*X*-cut	0.22
Sulser *et al.* (Ref. 23)	*X*- and *Y*-cuts	0.07–0.22
Xu *et al.* (Ref. 24)	*X*-cut	0.13–0.19

TABLE II. Table listing important parameters used to model LN in our SRIM simulations to obtain an estimate of material removal rate of LN using the FIB.

Parameter	Value used
Density	4.628 g/cm^3
Heat of sublimation for Li	1.67 eV
Heat of sublimation for Nb	7.59 eV
Heat of sublimation for O	2 eV
Surface binding energy	3.8 eV

our SRIM simulations. In comparison, Liu *et al.*[25] reported a material removal rate of 0.3 μm^3/nC using a similar SRIM simulation method to ours. However, in their paper, they have reported using a density of 9.45×10^{22} atoms/cm^3 or 23.2 g/cm^3 compared with the more realistic density for LN of 4.628 g/cm^3 that we have used.

In addition, our experimental material removal rate (0.30–0.34 μm^3/nC) is also in good agreement with the material removal rate we obtained from our SRIM simulations (0.37 μm^3/nC). We attribute the slight difference to the fact that the SRIM simulations do not take the geometry, specifically the aspect ratios, of the milled structures into account.

C. FIB milling of microchannels for microfluidics

Next, we investigated the milling characteristics of microchannels in *Y*-cut LN, which is the preferred orientation for SAW-based microfluidics applications. Channels with a fixed length of 10 μm and widths of 1 μm and 0.5 μm, were milled with varying dose at three different ion beam currents to investigate the material removal rate and profile of channels milled. The dimensions of each milled channel were then measured by the SEM after cross-sectioning the channel using the FIB as described in Sec. II. Figure 3(a) shows a plot of the milled volume as a function of ion dose for 10 μm long channels with widths of 1 μm and 0.5 μm milled using ion beam currents of 93, 460, and 2800 pA.

Both sets of channels (i.e., with 1 μm and 0.5 μm width) showed a linear trend of milled volume as a function of ion dose for low ion doses in good agreement with the theoretical value obtained from the SRIM simulation. At high ion doses, the milled volume decreased from this linear trend, indicating that the material removal rate became slower at high ion doses. In addition, we also observed that the cross-sectional profile of the milled channels varied significantly as a function of ion dose as shown in Figure 3(b). At low ion doses, the milled channels were almost perfectly rectangular in cross-section with only slightly sloping sidewalls as shown in Figure 3(b)(i) and (b)(iv). However, as the ion dose increased, and consequently the aspect ratio of the milled channel increased, the sidewalls of the channels became increasingly sloping (Figure 3(b)(ii) and (b)(v)), to the point where at the highest doses, the channels were entirely V-shaped (Figure 3(b)(iii) and (b)(vi)). For comparison, the cross-sectional profiles we obtain for various ion doses are similar to those obtained by Kim[37] and co-workers, who performed their work on silicon. These results indicate to us that material removal rate of LN is high at low ion dose (i.e., low aspect ratio) and that the material removal rate decreases as the ion dose of the milled channels increases.

TABLE III. Table listing sputter yield results obtained in our SRIM simulations of FIB milling of LN.

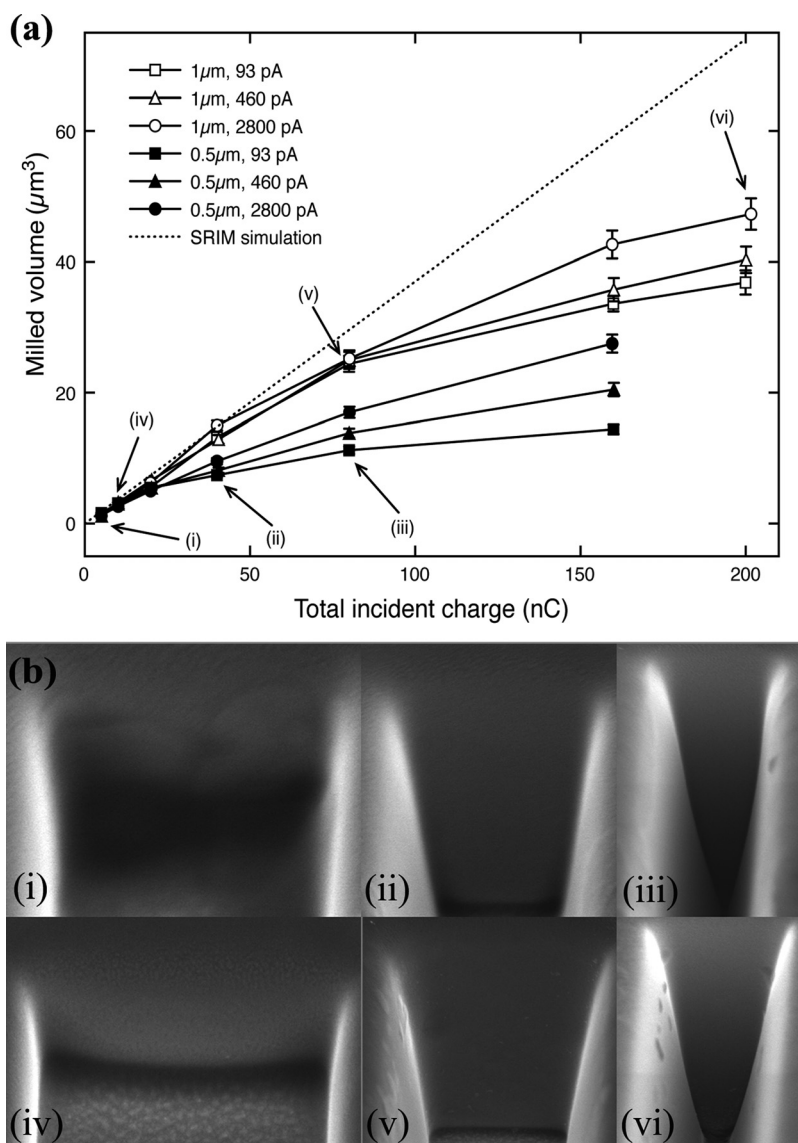| Atom type	Sputter yield (atoms/ion)
Li	1.87
O	5.38
Nb	0.69

FIG. 3. (a) Plot of milled volume as a function of incident ion dose for two sets of 10 μm long channels—1 μm wide and 0.5 μm wide—at three different ion beam currents. The symbols indicate data points, the solid lines act as a guide for the eye, and the dotted line represents the prediction obtained by SRIM simulations. (b) Characteristic sidewall profiles obtained by SEM for the following: (i) 0.5 μm wide channel at 10 nC ion dose, (ii) 0.5 μm wide channel at 40 nC ion dose, (iii) 0.5 μm wide channel at 80 nC ion dose, (iv) 1 μm wide channel at 20 nC ion dose, (v) 1 μm wide channel at 80 nC ion dose, and (vi) 1 μm wide channel at 200 nC ion dose.

Furthermore, at high ion doses (>100 nC), we observe that slightly more material is removed at a higher ion current compared to a lower ion current for the same total ion dose. For example, at an ion dose of 200 nC, 47 μm^3 of LN is removed at 2800 pA compared with 37 μm^3 at 93 pA. This suggests that material removal is more efficient at higher ion currents, where more ions strike the surface per second, for high aspect ratio structures as expected. However, the disadvantage of milling channels at high ion currents is that the lateral resolution of the milled channels will be lower because ion beam diameter is much larger than at low ion currents. For example, the ion beam diameter is quoted by the manufacturer to be approximately three times larger at 2800 pA (66 nm) than at 93 pA (24 nm). Consequently, the lateral resolution of sub-micron features milled using high ion currents will be lower than those milled at low ion currents.

D. Dependence of material removal rate on aspect ratio of milled structures

We have shown that material redeposition plays a significant role in the volume of material removed from channels and the cross-sectional profile of milled channels. To understand the quantitative effect of material redeposition on the material removal rate, we investigated the material removal rate in the FIB obtained for Y- and Z-cut LN samples as a function of aspect ratio of milled channels, where we define aspect ratio as the ratio of depth to width of structures milled, and compared our results with those obtained by other researchers. We kept the ion beam current and milling time fixed at 2.8 nA and 242 s, respectively, to ensure that the charge incident on each of the different structures was constant. The ion beam overlap was kept constant at 50% as before to minimize the effect of the Gaussian profile of the ion beam on the profile of the milled channels. We varied the aspect ratio of the structures milled from about 0.4–7 by varying the depth and width of the channels, while adjusting the length accordingly to keep the total expected volume of the milled channels constant. The depth and width of the channels were varied between 1 and 10 μm, while the length of the channels ranged from 10 to 25 μm. Subsequently, we milled cross-sections of each channel in the FIB, similar to that shown in Figure 1, and measured the dimensions of the milled channels using the SEM. Since we are directly measuring the dimensions of the cross-section of the milled channels, we are in effect taking into account any effect that the Gaussian profile of the ion beam may have on the profile of the milled channels.

Figure 4 shows the plot of material removal rate observed in the FIB as a function of the aspect ratio of milled channels. The material removal rate for each channel was calculated by dividing the total milled volume, as measured using the SEM, by the total charge incident on the channel (i.e., 2.8 nA × 242 s = 677.6 nC.) Previously published FIB milling results for LN, as shown in Table I, are also shown in Figure 4 for comparison.

From Figure 4, we observe that the material removal rate in the FIB is in good agreement with the theoretical value obtained from our SRIM simulation for low aspect ratio structures. This is because material redeposition is not a significant factor in this regime. We also observe that the material removal rate decreases as a function of aspect ratio of the milled structures, decreasing to approximately 50% of the initial material removal rate at aspect ratios greater than 4. In fact, our experimental data observed at aspect ratios greater than 2 agree well with
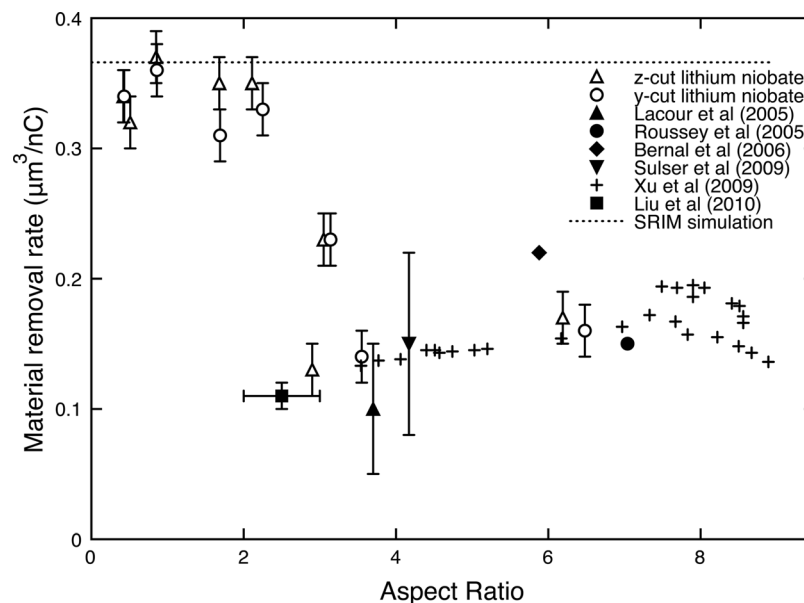

FIG. 4. Plot of the material removal rate observed as a function of aspect ratio of the milled channels for Y- and Z-cuts LN. Our experimental data points are represented by the hollow symbols, and results previously reported in the literature are represented by the filled symbols.

previously published experimental results. The reason for this decrease in material removal rate at high aspect ratios can be attributed to material redeposition.[33–35] It becomes more and more difficult to remove material from a deep yet narrow (i.e., high aspect ratio) structure because the material has to be expelled a long way to escape the top surface of the substrate, and there is a high probability that the material will be redeposited along the sidewalls within the structure itself. Alternatively, we can also explain the reduced material removal rate observed for high aspect ratio structures kinematically. For high aspect ratio structures, the surface atoms ejected from one sidewall of the milled structure are in closer proximity to the neighbouring sidewall than for low aspect ratio structures. Thus, the probability for collisions between sputtered atoms and between sputtered and surface atoms is higher for high aspect ratio structures, resulting in greater material redeposition and hence, a lower material removal rate. Consequently, the sidewalls of high aspect ratio channels are likely to be tapered, and we have experimentally observed this trend. One of the features of the FIB is its ability to fabricate high aspect ratio structures, and, therefore, a possible explanation for the results in the literature is the tendency for investigators to use this capability of the FIB, inadvertently reducing the reported material removal rate due to redeposition.

Figure 5 shows a SEM image of the cross-section of a typical high aspect ratio (aspect ratio = 2.7) channel in LN. As can be seen from the figure, the channel walls are V-shaped, which suggests that it is quite difficult to remove material from the bottom of this high aspect ratio channel due to material redeposition.[33–35] Consequently, in this case, milling any deeper than about 3 μm in depth does not result in any further increase in the depth of the structure actually milled.

E. Nanochannel fabrication and future work

Finally, we milled a nanochannel in a *Y*-cut sample, typically used in microfluidics experiments, to show our capability to fabricate nanochannels directly onto LN samples. Figure 6 shows a SEM image of a cross-section of a typical nanochannel (width = 100 nm, depth = 100 nm, and aspect ratio = 1) that we are able to routinely mill directly onto a LN sample. Unlike in the previous works involving FIB milling of lithium niobate,[19,21–25] the nanochannels we are fabricating are low aspect ratio structures (aspect ratio ≈ 1) and hence, we are able to utilise the higher material removal rate of lithium niobate in this regime to our advantage. Preliminary atomic force microscopy (AFM) measurements have indicated that the sidewall roughness of these FIB-milled nanochannels is less than 2 nm and that the sidewall profile of these channels may be slanted.
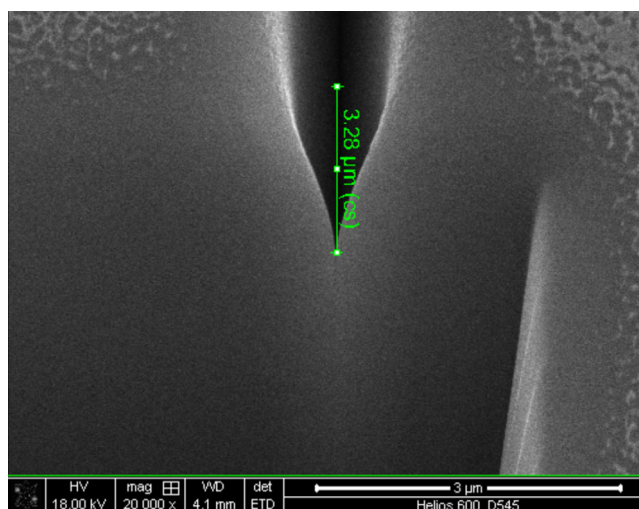

FIG. 5. SEM image of a sample cross-section of a FIB-milled high aspect ratio channel in *Z*-cut LN. The aspect ratio for this particular channel is 2.7.
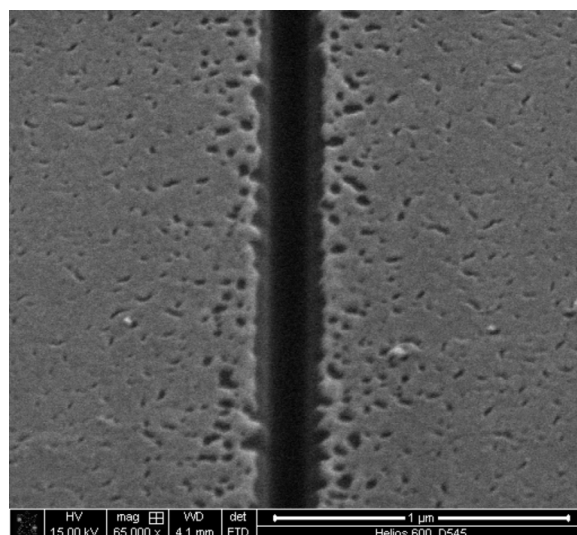
FIG. 6. SEM image of a cross-section of a FIB-milled nanochannel in *Y*-cut LN. This particular channel is roughly 100 nm wide and deep, and showcases our ability to directly mill nanochannels on LN samples.

In addition, preliminary experiments of imaging fluid inside such a FIB-milled nanochannel show that it is possible to image fluid containing fluorescent nanoparticles inside these nano-channels. Figure 7 shows a confocal microscope image of 22 nm fluorescent nanoparticles suspended in deionised water inside a FIB-milled nanochannel.

1 μl of the fluid containing the fluorescent nanoparticles was injected close to one end of the FIB-milled nanochannel and the sample was imaged in a Nikon A1 Rsi-MP confocal micro-scope after the fluid had mostly evaporated away. As seen in Figure 7, the fluid appeared to fill slightly more than half the length of the nanochannel through capillary action. Hence, we are confident of reproducibly milling structures down to the 100 nm regime as shown in Figure 6, and plan to use these devices to investigate SAW-driven nanoscale fluid flow in the future.

IV. CONCLUSIONS

In this paper, we have reported the experimental and simulation results for FIB milling of microchannels in LN. We compared two different cuts of LN, *Y*- and *Z*-cuts and found no sig-nificant difference in the experimental material removal rate in the FIB for the *Y*-cut samples compared with the *Z*-cut samples. The experimental material removal rate for both types of samples was about 0.3 μm^3/nC, about two times greater than the average material removal rate
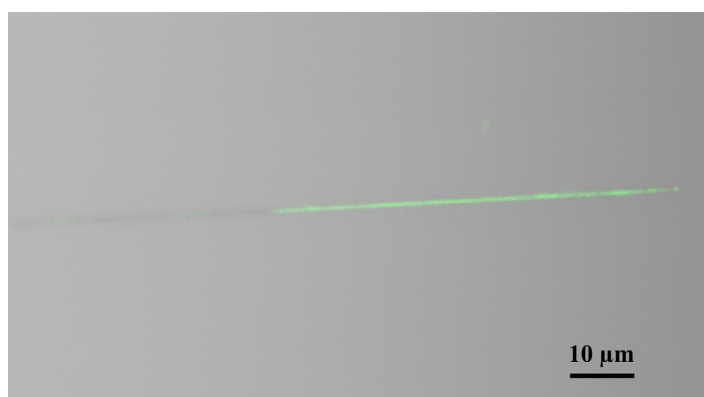

FIG. 7. Confocal microscope image of 22 nm fluorescent nanoparticles suspended in deionised water inside a FIB-milled nanochannel.

reported previously in the literature but in good agreement with the theoretical material removal rate obtained from SRIM simulations.

Next, we characterised the FIB milling process for $10\,\mu$m long microchannels with widths of $1\,\mu$m and $0.5\,\mu$m at three different ion currents, and shown that as the ion dose increases, the material removal rate decreases and the shape of the milled channels changes from rectangular to V-shaped. We attribute this decrease in material removal rate with increasing ion dose to the increasing significance in material redeposition as the milled structure gets deeper.

Hence, we proceeded to quantitatively show that the material removal rate in the FIB decreases as a function of the aspect ratio of the milled structures, likely due to the increased significance of material redeposition for high aspect ratio structures. In the low aspect ratio regime, the experimental material removal rate is in good agreement with the value obtained from SRIM simulations, and in the high aspect ratio regime, the material removal rate decreases by about a factor of two. In fact, in the high aspect ratio regime, our experimental results agree quite well with previous experimental results reported in the literature, which have solely focused on fabricating high aspect ratio structures in lithium niobate using the FIB milling technique.

Finally, we have showcased our ability to fabricate nanochannels with low aspect ratio on LN, taking advantage of the higher material removal rate of lithium niobate in this regime. Given the material removal rate we have observed ($0.3\,\mu$m^3/nC), the typical milling time for a single nanochannel that is $100\,\mu$m long, 100 nm wide, and 100 nm deep is approximately 30 s. Allowing for the time taken for sputtering the thin gold conducting layer, machine pumpdown and venting, we are able to process a single fluidic chip easily in under 3 h. We have also shown that it is possible to image fluid containing fluorescent nanoparticles inside these FIB-milled nanochannels using confocal microscopy. Our results will enable us to rapidly fabricate nanochannels directly on LN SAW devices, which will minimise any losses in intensity and coupling of the surface acoustic waves, and we plan to investigate nanoscale fluid flow by integrating these nanochannels onto LN SAW devices in the future.

ACKNOWLEDGMENTS

[1]K. Hashimoto, *Surface Acoustic Wave Devices in Telecommunications: Modelling and Simulation* (Springer, New York, 2000).

[2]C. Campbell, *Surface Acoustic Wave Devices for Mobile and Wireless Communications* (Academic, NY, 1998) p. 631.

[3]J. Friend and L. Yeo, *Piezoelectric Materials for Microfluidics (Encyclopedia of Micro- and Nanofluidics)*, edited by D. Li (Springer, New York, 2008), Vol. 1, pp. 1654–1662.

[4]J. Campbell and W. Jones, IEEE Trans. Sonics Ultrason. **15**, 209 (1968).

[5]W. Sohler, Thin Solid Films **175**, 191 (1989).

[6]L. K. Oxenløwe, F. Gómez-Agis, C. Ware, S. Kurimura, H. C. H. Mulvad, M. Galili, H. Nakajima, J. Ichikawa, D. Erasme, A. T. Clausen, and P. Jeppesen, J. Lightwave Technol. **27**, 205 (2009).

[7]J. Friend and L. Yeo, Rev. Mod. Phys. **83**, 647 (2011).

[8]L. Y. Yeo and J. R. Friend, Biomicrofluidics **3**, 012002 (2009).

[9]L. Y. Yeo, J. R. Friend, M. P. McIntosh, E. N. Meeusen, and D. A. Morton, Expert Opin. Drug Deliv. **7**, 663 (2010).

[10]A. Qi, J. Friend, L. Yeo, D. Morton, M. McIntosh, and L. Spiccia, Lab Chip **9**, 2184 (2009).

[11]M. K. Tan, J. Friend, and L. Y. Yeo, Phys. Rev. Lett. **103**, 024501 (2009).

[12]H. Li, J. Friend, and L. Yeo, Biomed. Microdevices **9**, 647 (2007).

[13]M. Tan, L. Yeo, and J. Friend, Europhys. Lett. **87**, 47003 (2009).

[14]R. Shilton, M. K. Tan, L. Yeo, and J. R. Friend, J. Appl. Phys. **104**, 014910 (2008).

[15]J. Friend, L. Yeo, D. Arifin, and A. Mechler, Nanotechnology **19**, 145301 (2008).

[16]M. Alvarez, L. Y. Yeo, J. R. Friend, and M. Jamriska, Biomicrofluidics **3**, 014102 (2009).

[17]H. Li, J. Friend, L. Yeo, A. Dasvarma, and K. Traianedes, Biomicrofluidics **3**, 034102 (2009).

[18]H. Li, J. R. Friend, and L. Y. Yeo, Biomaterials **28**, 4098 (2007).

[19]F. Lacour, N. Courjal, M.-P. Bernal, A. Sabac, C. Bainier, and M. Spajer, Opt. Mater. **27**, 1421 (2005).

[20]V. Laude, M. Wilm, S. Benchabane, and A. Khelif, Phys. Rev. E **71**, 36607 (2005).

[21]M. Roussey, M.-P. Bernal, N. Courjal, and F. I. Baida, Appl. Phys. Lett. **87**, 241101 (2005).

[22]M.-P. Bernal, N. Courjal, J. Amet, M. Roussey, and C. H. Hou, Opt. Commun. **265**, 180 (2006).

[23]F. Sulser, G. Poberaj, M. Koechlin, and P. Günter, Opt. Express. **17**, 20291 (2009).

[24]X. Xu, S. Yan, J. Xue, Y. Wang, K. Wang, and X. Wang, J. Vac. Sci. Technol. B. **27**, 1851 (2009).

[25]P. Liu, Q. Huang, X.-L. Wang, X. Xu, and S. Yan, J. Korean Phys. Soc. **56**, 1369 (2010).

[26]J. Edel, J. Edel, and A. De Mello, *Nanofluidics: Nanoscience and Nanotechnology* (Royal Society of Chemistry, Cambridge, 2009).

[27]M. Whitby and N. Quirke, Nat. Nanotechnol. **2**, 87 (2007).

[28]Z. Insepov, D. Wolf, and A. Hassanein, Nano Lett. **6**, 1893 (2006).

[29]P. Nassoy, D. Cuvelier, R. Bruinsma, and F. Brochard-Wyart, Europhys. Lett. **84**, 18004 (2008).

[30]M. Shannon, P. Bohn, M. Elimelech, J. Georgiadis, B. Mariñas, and A. Mayes, Nature (London) **452**, 301 (2008).

[31]D. M. Karabacak, V. Yakhot, and K. L. Ekinci, Phys. Rev. Lett. **98**, 254505 (2007).

[32]J. F. Ziegler, J. P. Biersack, and U. Littmark, *The Stopping and Range of Ions in Solids* (Pergamon, NY, 1985).

[33]B. I. Prenitzer, C. A. Urbanik-Shannon, L. A. Giannuzzi, S. R. Brown, R. B. Irwin, T. L. Shofner, and F. A. Stevie, Microscopy Microanal. **9**, 216 (2003).

[34]*Introduction to Focused Ion Beams—Instrumentation*, *Theory*, *Techniques and Practice* edited by L. A. Giannuzzi and F. A. Stevie (Springer, New York, 2005).

[35]W. J. MoberlyChan, J. Phys: Condens. Matter **21**, 224013 (2009).

[36]R. S. Weis and T. K. Gaylord, Appl. Phys. A **37**, 191 (1985).

[37]H. B. Kim, G. Hobler, A. Lugstein, and E. Bertagnolli, J. Micromech. Microeng. **17**, 1178 (2007).